PCP
PLANT & CELL PHYSIOLOGY

The Chaperone NASP Contributes to de Novo Deposition of the Centromeric Histone Variant CENH3 in *Arabidopsis* Early Embryogenesis

Hidenori Takeuchi[1,2,*], Shiori Nagahara[1], Tetsuya Higashiyama[1,3,4] and Frédéric Berger[5]

[1]Institute of Transformative Bio-Molecules (WPI-ITbM), Nagoya University, Nagoya, Aichi 464-8601, Japan
[2]Institute for Advanced Research, Nagoya University, Nagoya, Aichi 464-8601, Japan
[3]Division of Biological Science, Graduate School of Science, Nagoya University, Nagoya, Aichi 464-8602, Japan
[4]Department of Biological Sciences, Graduate School of Science, The University of Tokyo, Tokyo 113-0033, Japan
[5]Gregor Mendel Institute, Austrian Academy of Sciences, Vienna BioCenter, Vienna 1030, Austria

*Corresponding author: E-mail, hidenori.takeuchi@itbm.nagoya-u.ac.jp
(Received 8 October 2023; Accepted 25 March 2024)

Regular Paper

The centromere is an essential chromosome region where the kinetochore is formed to control equal chromosome distribution during cell division. The centromere-specific histone H3 variant CENH3 (also called CENP-A) is a prerequisite for the kinetochore formation. Since CENH3 evolves rapidly, associated factors, including histone chaperones mediating the deposition of CENH3 on the centromere, are thought to act through species-specific amino acid sequences. The functions and interaction networks of CENH3 and histone chaperons have been well-characterized in animals and yeasts. However, molecular mechanisms involved in recognition and deposition of CENH3 are still unclear in plants. Here, we used a swapping strategy between domains of CENH3 of *Arabidopsis thaliana* and the liverwort *Marchantia polymorpha* to identify specific regions of CENH3 involved in targeting the centromeres and interacting with the general histone H3 chaperone, nuclear autoantigenic sperm protein (NASP). CENH3's LoopN-α1 region was necessary and sufficient for the centromere targeting in cooperation with the α2 region and was involved in interaction with NASP in cooperation with αN, suggesting a species-specific CENH3 recognition. In addition, by generating an *Arabidopsis nasp* knock-out mutant in the background of a fully fertile *GFP-CENH3/cenh3-1* line, we found that NASP was implicated for de novo CENH3 deposition after fertilization and thus for early embryo development. Our results imply that the NASP mediates the supply of CENH3 in the context of the rapidly evolving centromere identity in land plants.

Keywords: *Arabidopsis thaliana* ● Centromere-specific histone H3 (CENH3) ● Embryogenesis ● Histone chaperone ● Nuclear autoantigenic sperm protein (NASP)

Introduction

In nuclei of eukaryotic cells, DNA is organized into chromatin that consists of an array of nucleosomes and associated proteins. The nucleosome, a basic unit of chromatin, is formed with ∼150-bp DNA and four core histones, H2A, H2B, H3 and H4 (Luger et al. 1997). Most eukaryote species possess a set of variants for each core histone, so-called histone variants, and use them to confer specific properties on each genomic region (Pusarla and Bhargava 2005, Talbert and Henikoff 2010, Kawashima et al. 2015, Jiang and Berger 2017a). The histone monomer consists of the histone-fold domain, which contains α-helices connected by loops and mediates histone–histone and histone–DNA interaction, and the unstructured N- and C-terminal tails, which protrude from the nucleosome core particle and generally undergo covalent modifications, including methylation, acetylation, phosphorylation and ubiquitination (Luger et al. 1997, Khorasanizadeh 2004).

The histone variants H3.1 and H3.3 are incorporated into nucleosomes of non-centromeric chromatin during DNA replication and throughout the cell cycle, respectively (Filipescu et al. 2013, Talbert and Henikoff 2017, Borg et al. 2021). The histone variant CENH3 specifically marks the centromere. Due to the importance of CENH3 targeting to the centromere in eukaryotes, regulatory factors and DNA sequences related to CENH3 deposition as well as their evolution have been extensively studied in yeast, animals and plants (Malik et al. 2002, Talbert et al. 2002, Henikoff and Dalal 2005, Morris and Moazed 2007, Zhang et al. 2008, Hirsch et al. 2009, Malik and Henikoff 2009, Nagaki et al. 2010, Yuan et al. 2015, Maheshwari et al. 2017, Rosin and Mellone 2017, Naish et al. 2021). In eukaryotes, the deposition of CENH3 proteins, also called CENP-A in mammals,

Plant Cell Physiol. 65(7): 1135–1148 (2024) doi:https://doi.org/10.1093/pcp/pcae030, Advance Access publication on 10 April 2024, available online at https://academic.oup.com/pcp

CID (for centromere identifier) in flies, Cse4 in budding yeast *Saccharomyces cerevisiae* and Cnp1 in fission yeast *Schizosaccharomyces pombe*, is required for proper point kinetochore formation and thus equal chromosome distribution to daughter cells after cell division. In contrast to other H3 variants, the amino acid sequences of CENH3 proteins are variable among species, even close relatives (Malik et al. 2002, Nagaki et al. 2010, Sanei et al. 2011, Rosin and Mellone 2016). Similarly, both centromeric DNA repeats and centromeric/heterochromatic proteins evolve rapidly.

In contrast to relatively conserved canonical H3s, rapidly evolving CENH3 proteins are recognized by distantly related or non-conserved histone chaperones, HJURP in mammals, Scm3 in yeasts and CAL1 in flies (Camahort et al. 2007, Stoler et al. 2007, Dunleavy et al. 2009, Foltz et al. 2009, Zhou et al. 2011, Phansalkar et al. 2012, Chen et al. 2014). In humans and yeasts, the chaperones HJURP and Scm3 recognize the loop 1 and α2 helix (designated as the CENP-A targeting domain, CATD) within the histone-fold domain of CENH3 (CENP-A/Cse4) (Cho and Harrison 2011, Bassett et al. 2012). In *Drosophila* species, CAL1 distinguishes *Drosophila* CENH3 homologs via loop 1 in a species-specific manner (Rosin and Mellone 2016). HJURP, Scm3 and CAL1 chaperones specifically interact with CENH3 and mediate de novo CENH3 deposition via the self-sustaining epigenetic mechanism, which maintains centromere positioning and occasionally creates novel centromeres (Barnhart et al. 2011, Roure et al. 2019, Medina-Pritchard et al. 2020, Palladino et al. 2020). Similar to these features of animals and yeasts, it is suggested that in plants CENH3 recognition depends on its species-specific sequence and that CENH3 deposition is mediated by a yet uncharacterized self-sustaining mechanism (Ravi et al. 2010, Maheshwari et al. 2015, Marimuthu et al. 2021). In flowering plants (angiosperms), failure of CENH3 deposition and function leads to uniparental genome elimination after fertilization and consequently to generation of haploid individuals, which is utilized as doubled haploid technology to rapidly obtain homozygous lines (Ravi and Chan 2010, Ravi et al. 2014). Therefore, the molecular mechanisms involved in CENH3 recognition and deposition have been intensively studied in crop species as well as in *Arabidopsis thaliana* (Lermontova et al. 2006, Ingouff et al. 2010, Sanei et al. 2011, Karimi-Ashtiyani et al. 2015, Kuppu et al. 2020). However, our knowledge about the requirements for recognition and deposition of plant CENH3 is still limited.

A homolog of nuclear autoantigenic sperm protein (NASP) in *A. thaliana* is also characterized as a common histone H3 chaperone (Maksimov et al. 2016, Le Goff et al. 2020). NASP is a tetratricopeptide repeat (TPR)–containing protein conserved in a wide range of eukaryotes and is involved in various cellular events, such as DNA replication, cell proliferation, cell growth and embryonic development in mammals (Richardson et al. 2000, 2006, Dunleavy et al. 2007, Finn et al. 2012). NASP binds to H3–H4 dimers to reserve them in the soluble/non-nucleosomal fraction and hand off them to chromatin assembly factors, suggesting the function of histone supply chain for the demand in mammalian cells (Campos et al. 2010, Cook et al. 2011). Human NASP protein possesses the direct nucleosome assembly activity toward CENH3 (CENP-A) as well as the canonical H3.1 and H3.3 in vitro (Osakabe et al. 2010). In *S. pombe*, NASP (called as Sim3) binds to CENH3 (Cnp1) and is required for its deposition on centromere (Dunleavy et al. 2007). Recent studies in *A. thaliana* have identified NASP as an interactor of both H3.3 and CENH3 through co-immunoprecipitation and mass spectrometry analysis using *A. thaliana* tissues or cultured cell line (Maksimov et al. 2016, Le Goff et al. 2020). Similar to yeast and human NASPs, *A. thaliana* NASP is broadly expressed in actively dividing tissues and is a soluble protein localized at the nucleoplasm. In vitro experiments using purified histones and NASP have demonstrated that *A. thaliana* NASP binds monomeric H3.1 and H3.3 as well as H3.1–H4 and H3.3–H4 dimers, but not monomeric H4, stabilizes H3–H4 tetramers from H3–H4 dimers and promotes tetrasome formation with DNA (Maksimov et al. 2016). Interaction assay using a bimolecular fluorescence complementation (BiFC) have suggested that *A. thaliana* NASP interacts with both the N-terminal tail and the histone-fold domain of CENH3 *in planta* (Le Goff et al. 2020). Knockdown of *NASP* expression causes moderate reduction in nuclear CENH3 levels and ~30% reduction in CENH3 signal at the centromere (Le Goff et al. 2020).

Here, we show large-scale and detailed structure–function analysis of plant CENH3 in terms of centromere targeting in *A. thaliana* cells and investigate NASP function in *A. thaliana* embryogenesis by generating a *nasp* knock-out mutant. By a domain swapping strategy using CENH3 proteins of *A. thaliana* and the liverwort *Marchantia polymorpha*, we reveal the requirement of specific CENH3 regions, such as LoopN-α1 region, for centromere targeting and interaction with NASP in a lineage-specific manner. Additionally, we characterize the role of NASP in de novo CENH3 deposition after fertilization.

Results and Discussion

Targeting of *A. thaliana* centromeres by CENH3 protein involves its angiosperm-specific amino acid sequence context

To understand a lineage-specific recognition mechanism of plant CENH3 proteins for the centromere targeting, we compared CENH3 amino acid sequences between the dicot *A. thaliana* (HTR12; AtCENH3), the monocot *Zea mays* (ZmCENH3) that has been previously shown to target *A. thaliana* centromeres (Ravi et al. 2010), the liverwort *M. polymorpha* (MpCENH3) and human (CENP-A) (**Fig. 1A** and **Supplementary Fig. S1**). In contrast to the canonical H3.3 histones, which share the same amino acid sequences between *A. thaliana* and *M. polymorpha* and have only six amino acid differences between human and land plants (**Supplementary Fig. S1A**), CENH3 proteins are highly variable (**Fig. 1A**) as illustrated previously (Ravi et al. 2010). The N-terminal tail of CENH3 proteins is especially hypervariable with different lengths, in

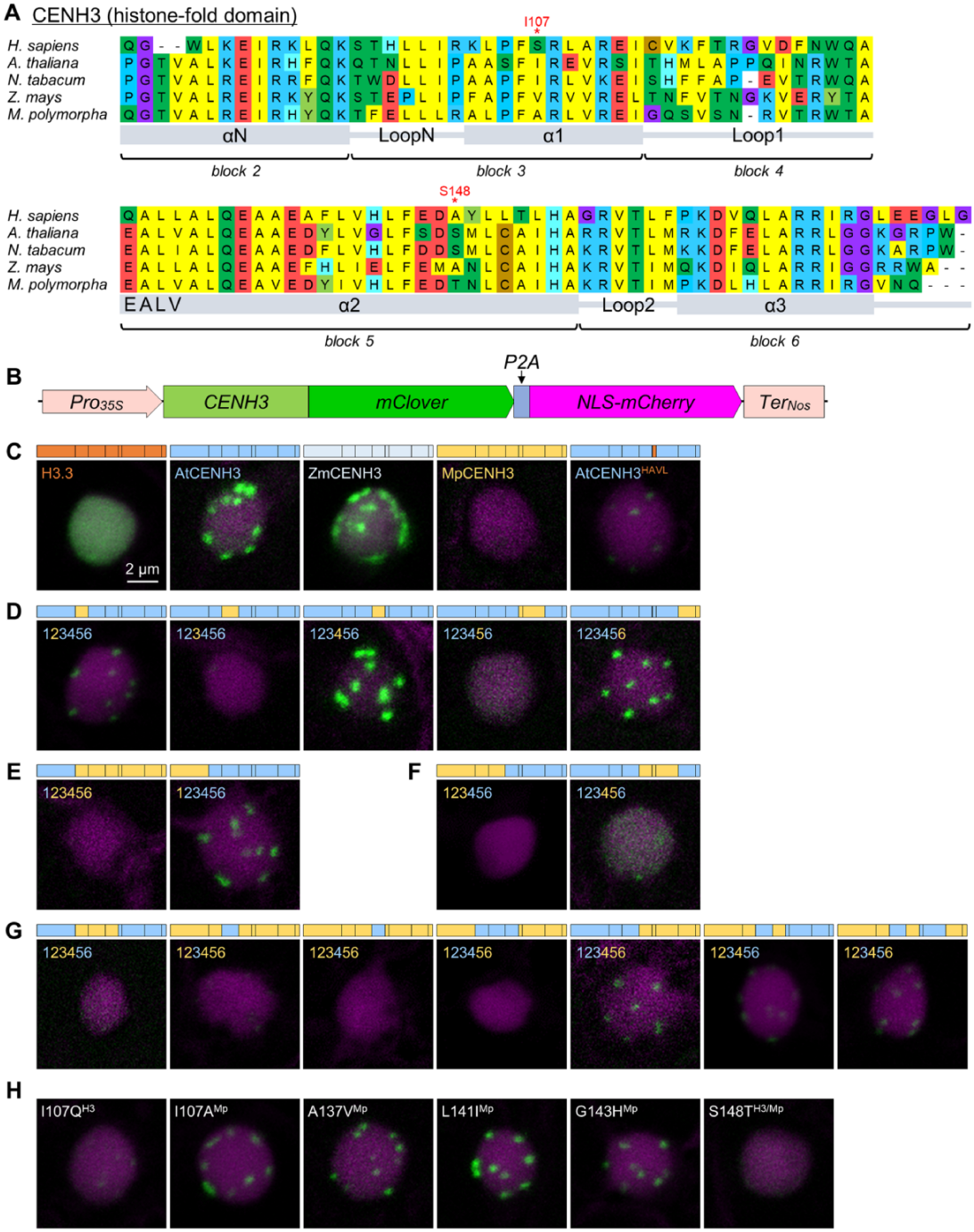

Fig. 1 CENH3 protein regions required for centromere targeting in *A. thaliana*. (A) Sequence alignment of the histone-fold domain of *H. sapiens*, *A. thaliana*, *N. tabacum*, *Z. mays* and *M. polymorpha* CENH3 proteins. The protein secondary structure and blocks dividedly analyzed in this study are shown below the alignment. See also **Supplementary Fig. S1A** and **B** for sequence alignments of the canonical H3 and N-terminal tail of CENH3. (B) Schematic of the expression construct to produce CENH3 variants fused to mClover and NLS-mCherry from a single transcript. Co-translational 'self-cleavage' during translation of the 2A peptide sequence (*P2A*) results in the generation of two separate proteins. (C–H) Localization assessment of CENH3 variants in the *A. thaliana* petal cell. Block bars drawn above each image and labels indicate the protein structure of each variant with colors. Each figure panel consisting of multiple variants represents comparisons examining canonical H3 (H3.3), CENH3 of *A. thaliana* (AtCENH3), *Z. mays* (ZmCENH3), *M. polymorpha* (MpCENH3) and AtCENH3 substituted with HAVL (AtCENH3^{HAVL}) (C); required single AtCENH3 region (D); importance of the N-terminal tail (E) and CATD (F); sufficient AtCENH3 region (G); and required amino acid of AtCENH3 (H). The images are representative nuclei from more than three images capturing multiple nuclei. See also **Supplementary Fig. S2** and **S3** for a summary of this assay and representative images of a similar assay using tobacco BY-2 cells.

contrast to the strong degree of conservation of the histone-fold domain (**Fig. 1A** and **Supplementary Fig. S1B**).

Previous studies have shown that CENH3 proteins from angiosperms, including several *Brassicaceae* species, the grapevine *Vitis vinifera* and the monocot *Z. mays*, are able to target *A. thaliana* centromeres and to complement the embryo lethality of *cenh3-1* null mutation when expressed without the GFP tag (Ravi et al. 2010, Maheshwari et al. 2015). The histone-fold domain of CENH3 is sufficient to target the centromere (Ravi and Chan 2010). To obtain further insight into the sequence specificity for the CENH3 function, we used the MpCENH3 sequence of the distant land plant *M. polymorpha*, which is substantially different from *A. thaliana* CENH3 in the histone-fold domain [58% (56/97), including gaps], even though ZmCENH3 is similarly different (58%, 57/98) (**Fig. 1A**). To assess the protein localization of CENH3 variants after virtually comparable translation levels in plant cells, we constructed an expression vector that consists of the *cauliflower mosaic virus 35S* promoter, *mClover* encoding the green fluorescent protein and *NLS-mCherry* for the nuclear-localized red fluorescent protein, connected by the *P2A* sequence for the 2A peptide from porcine teschovirus-1 (**Fig. 1B**). The P2A sequence causes co-translational 'self-cleavage' during translation as a result of ribosome skipping (Kawashima et al. 2014, Liu et al. 2017), which generates mClover-fused CENH3 variant and NLS-mCherry proteins from a single mRNA.

To obtain steady and reliable results, we generated transgenic *A. thaliana* individuals harboring a series of CENH3 variants and observed mClover and mCherry fluorescence in the petal, which contains actively dividing cells and is useful to capture fluorescence signals with a lower background (**Fig. 1C–H**). In NLS-mCherry-positive nuclei, AtCENH3-mClover and ZmCENH3-mClover marked dot-like centromere regions. As a control, the exchange of the four contiguous amino acids located at the N-terminal of α2 helix following loop 1, which distinguish CENH3, to another four amino acids (HAVL) from H3.3 caused a dramatic reduction in the mClover signal with only faint dot-like localization (**Fig. 1C**, AtCENH3^{HAVL}). Contrasting with AtCENH3 and ZmCENH3, MpCENH3-mClover signals were undetectable (**Fig. 1C**), suggesting that MpCENH3 misses an angiosperm-specific sequence necessary for its deposition on the centromeres.

CENH3 deposition on *A. thaliana* centromeres requires its LoopN-α1 region

We next sought to define specific regions of CENH3 important for the lineage-specific amino acid recognition in the *A. thaliana* cell. By generating a series of transgenic *A. thaliana*–expressing chimeric CENH3 proteins, which consist of each block from AtCENH3 and MpCENH3 (**Fig. 1A** and **Supplementary Fig. S2**), we evaluated the localization of each chimeric CENH3 protein. Swapping one block of AtCENH3 with that of MpCENH3 indicated that LoopN-α1 (block 3) and α2 (block 5) were required for targeting the *A. thaliana* centromere (**Fig. 1D**). The N-terminal tail from AtCENH3 was not required for centromere targeting of MpCENH3 (**Fig. 1E**), although the N-terminal tail is important for full CENH3 functions in *A. thaliana* (Ravi and Chan 2010, Maheshwari et al. 2015). In human cells, a domain spanning loop 1 to α2 (designated as CATD) of CENP-A conferred centromere targeting and function when swapped into canonical human H3 (Black et al. 2007). In contrast, a corresponding domain of AtCENH3 failed to complement *A. thaliana cenh3-1* phenotype when swapped into H3.3 (Ravi et al. 2010). We also assessed the impact of CATD (blocks 4 and 5) of AtCENH3 on localization in *A. thaliana* cells by using MpCENH3 as a donor. The CATD and a larger domain containing the CATD and the α3 region (block 6) of AtCENH3 were not sufficient for centromere targeting (**Fig. 1F** and **Supplementary Fig. S2**). By contrast, the mClover signal of a chimeric AtCENH3 having CATD of MpCENH3 was detected in the nucleus and weakly focused on dot-like regions resembling centromeres (**Fig. 1F** and **Supplementary Fig. S2**), suggesting that regions outside of CATD are involved in escort and reserve of plant CENH3 at the nucleoplasm through lineage-specific amino acid recognition.

To determine the regions sufficient for *A. thaliana* centromere targeting in the plant CENH3 framework, we analyzed additional chimeric CENH3 variants (**Fig. 1G**). In the presence of the LoopN-α1 (block 3) of AtCENH3, additional AtCENH3 regions, such as the N-terminal tail and αN regions (blocks 1 and 2) or α2 region (block 5), conferred the capability to target centromeres in a lineage-specific manner. We searched for the angiosperm CENH3-specific amino acids responsible for targeting *A. thaliana* centromeres and found that two AtCENH3 mutants possessing single amino acid substitution, I107Q and S148T, abolished centromere targeting (**Fig. 1H**).

To complement the results obtained in *A. thaliana* cells, we also observed tobacco BY-2-cultured cell lines harboring each chimeric CENH3 construct (**Supplementary Fig. S2** and **S3**). We obtained fundamentally similar results in the BY-2 system to the *A. thaliana* system: LoopN-α1 (block 3) of AtCENH3 was the necessary region for centromere targeting. The I107A mutant, which has a single substitution by the MpCENH3-type amino acid, abolished specific targeting to the centromere in the BY-2 nucleus, while the S148T mutant was localized to the centromere at a comparable level to wild-type AtCENH3 (**Supplementary Fig. S3**). Several amino acids in the LoopN-α1 and α2 regions are different between *A. thaliana* and tobacco (*Nicotiana tabacum*) CENH3 proteins (**Fig. 1A**; Nagaki et al. 2010), suggesting that endogenous CENH3 recognition factors of tobacco might recognize slightly different sequence contexts in these regions. In summary, using the swapping strategy with AtCENH3 and MpCENH3 sequences, we found that the CENH3 LoopN-α1 region in combination with additional regions, such as α2, is key for centromere targeting in *A. thaliana* and BY-2 cells, indicating a lineage-specific amino acid recognition mechanism for plant CENH3.

The general H3/CENH3 chaperone NASP contributes to embryogenesis in *A. thaliana*

Within the eukaryotic lineage, CENH3 is generally indispensable for centromere specification to form the kinetochore. However,

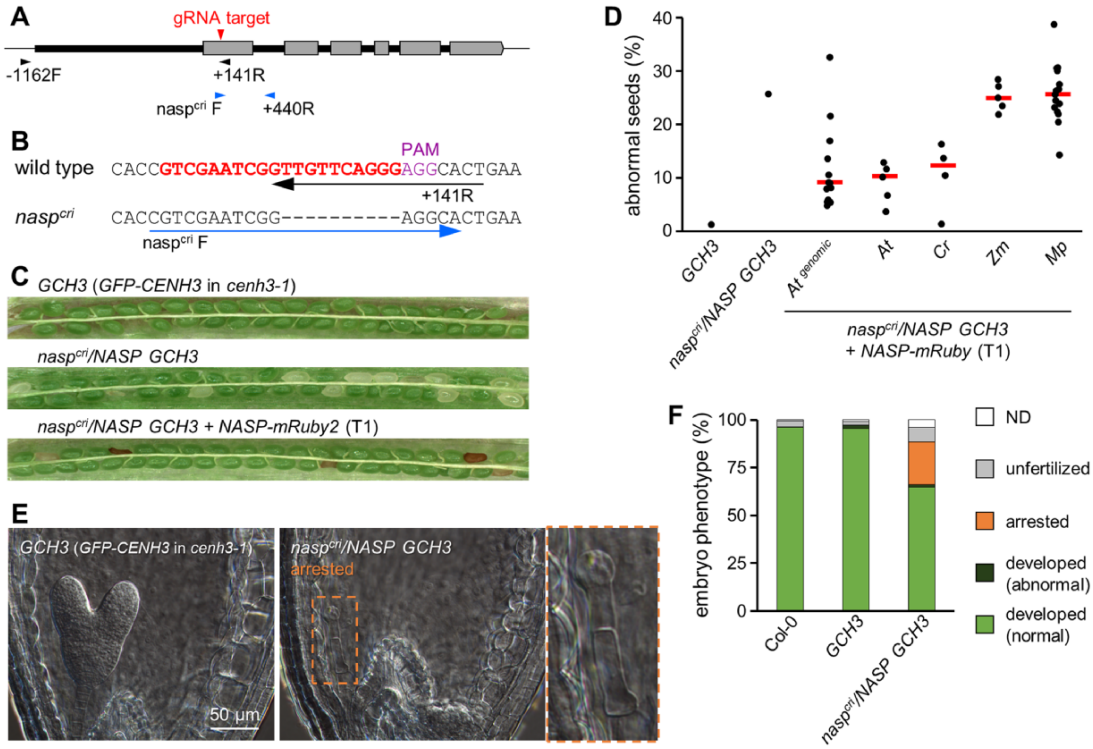

Fig. 2 Embryo lethal phenotype of the *nasp*^{cri} knock-out mutant in the *GCH3* line. (A) Schematic of the *NASP* gene structure with a guide RNA (gRNA) target site and genotyping primers. Boxes are exons of *NASP* gene. The bold line indicates a region used for complementation constructs. (B) Primer design to exclusively amplify the endogenous *NASP* gene and *nasp*^{cri} mutant allele. (C) Representative images of developing seeds in siliques of the *GCH3* background line (*GFP-CENH3* in *cenh3-1*), a heterozygous *nasp*^{cri}/*NASP* in *GCH3* and a complemented line with *NASP-mRuby2* transgene. (D) The percentage of abnormal seeds per developing seeds in self-pollinated siliques. For transgenic lines with the *nasp*^{cri}/*NASP* genotype, each dot represents the value for each independent T1 plant. Red bars indicate median values. Approximately 200 developing seeds were counted from five siliques. (E) Embryo development in *GCH3* or *nasp*^{cri}/*NASP GCH3* ovules 5 DAP. A heart-stage embryo in *GCH3* ovule and an early arrested embryo at one-cell stage in self-pollinated *nasp*^{cri}/*NASP GCH3* ovule. (F) The proportion of embryo phenotype. The phenotype was categorized based on observation as follows: developed (normal), about heart-stage embryo; developed (abnormal), globular to heart-stage embryo with distorted shape; arrested, one- or two-cell stage embryo; unfertilized, non-elongated egg cell or no egg cell structure due to degeneration; ND, not defined. A total of 209–321 ovules/seeds from four to six siliques were analyzed for each genotype.

despite this common function, CENH3 proteins have evolved rapidly. Consistent with this divergence, distantly related or non-conserved histone chaperones, such as HJURP in mammals, Scm3 in yeasts and CAL1 in flies, are species-specific chaperones for CENH3/CENP-A/Cse4/CID (Camahort et al. 2007, Stoler et al. 2007, Dunleavy et al. 2009, Foltz et al. 2009, Zhou et al. 2011, Phansalkar et al. 2012, Chen et al. 2014). Although no specific chaperones that specifically deposit CENH3 have been identified in the plant lineage, one of the histone chaperone homologues found in animals and yeasts, NASP, has been reported to be a general H3 chaperone that escorts CENH3 as well as H3.1 and H3.3 into the nucleoplasm in *A. thaliana* (Maksimov et al. 2016, Le Goff et al. 2020).

We initially tried to identify a novel specific chaperone that functions in species-specific CENH3 recognition by our reverse-genetic mini-screening of CENH3-related factors, including genes with unknown function co-expressed with *CENH3*, but we failed to obtain putative knock-out mutants showing embryo lethality similar to *cenh3* mutants. We also generated CRISPR/Cas9-mediated mutants for homologs of histone chaperones in the transgenic plant line *GCH3* that expresses *GFP-CENH3* in the *cenh3-1* mutant background (Ravi et al. 2010). We obtained a heterozygous 10-bp deletion mutant of *NASP* gene in line *GCH3* (*nasp*^{cri}/*NASP GCH3*) (**Fig. 2A, B**). The 10-bp deletion causes a frameshift and premature stop codon in the first exon of the *NASP* gene (**Supplementary Fig. S4**). A homozygous *nasp*^{cri} *GCH3* mutant was never obtained from progeny of the heterozygous line. In self-pollinated *nasp*^{cri}/*NASP GCH3* siliques, ∼25% of developing seeds were white embryoless seeds or collapsed brown seeds, indicative of the embryonic defect (**Fig. 2C, D**). About 22% of ovules in self-pollinated *nasp*^{cri}/*NASP GCH3* siliques had an arrested embryo at 1- to 2-cell stages, compared with ovules of wild-type Col-0 and *GCH3* containing a normal heart-stage embryo (**Fig. 2E, F**). This phenotype was complemented in more than half of T1 plants carrying the *NASPpro::NASP-mRuby2* (native promoter-driven genomic *NASP* fused with red fluorescent protein gene *mRuby2*) (**Fig. 2D**, *At*^{genomic}). From these results, we concluded

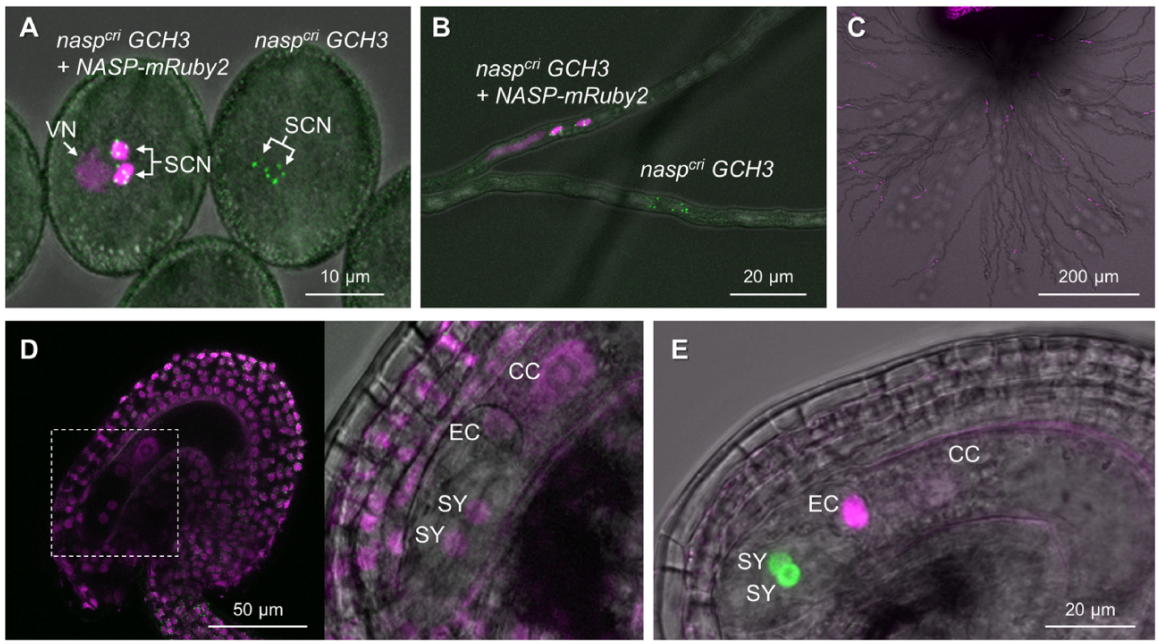

Fig. 3 Unaffected development and function of male and female gametophytes in *nasp*^{cri} *GCH3*. (A–C) In a plant line, *nasp*^{cri}/*nasp*^{cri} *GCH3* complemented with a hemizygous *NASPpro::NASP-mRuby2* transgene, indistinguishable development and GFP-CENH3 localization of pollen grains (A), equivalent growth ability of pollen tubes (B) and comparable wavy response to the AtLURE1 attractant peptide (500 nM in the pollen tube growth medium) of semi-in vivo growing pollen tubes (C) between *nasp*^{cri} pollen with and without NASP-mRuby2. (D) NASP-mRuby2 localization in the nuclei of the egg, central and synergid cells in the ovule. (E) Normal cell morphology and marker gene expression in *nasp*^{cri}/*nasp*^{cri} generated by backcross with FGR8.0 containing gene cassettes for the egg cell nucleus (*EC1.1pro::NLS-3xDsRed2*) and the synergid cell nucleus (*AtLURE1.2pro::NLS-3xGFP*) (Völz et al. 2013). VN, vegetative nucleus; SCN, sperm cell nucleus; EC, egg cell; CC, central cell; SY, synergid cell.

that the 10-bp deletion recessive mutation was responsible for the loss-of-function NASP and the observed embryogenesis defect in homozygous *nasp*^{cri} *GCH3* seeds. It should be noted that the completely arrested embryonic phenotype caused by the loss-of-function *nasp* mutation was masked in plants without the *cenh3-1* mutation and *GFP-CENH3* transgene, by backcrossing with wild-type Col-0. We obtained a homozygous *nasp*^{cri} mutant in the wild-type background showing normal vegetative growth as well as fertility (**Supplementary Fig. S5A**), implying that the GFP tag of CENH3 might interfere with the interaction with some other components important for the normal CENH3 supply network. Nevertheless, our results indicate that *NASP* is indispensable for *A. thaliana* development under a certain condition, at least in the *GCH3* background.

Male and female gametophytes appear to be unaffected by the *nasp*^{cri} mutation

Since *NASP* is broadly expressed in dividing cells, including reproductive tissues (Le Goff et al. 2020), we investigated the expression and contribution of NASP in male and female gametophytes. Pollen viability staining showed that pollen development in anthers of *nasp*^{cri}/*NASP GCH3*, as well as homozygous *nasp*^{cri} mutant with wild-type background, appeared to be normal, similar to *GCH3* (**Supplementary Fig. S5B**). Using a plant line with homozygous *nasp*^{cri} *GCH3* complemented by a hemizygous *NASPpro::NASP-mRuby2* transgene, we observed NASP-mRuby2 localization at the vegetative and sperm cell nuclei and centromere-localized GFP-CENH3 signals at the sperm cell nuclei, independent of the presence of NASP-mRuby2 (**Fig. 3A**). Pollen tube growth ability was equivalent between *nasp*^{cri} *GCH3* pollen tubes with and without NASP-mRuby2 protein (**Fig. 3B**). An important pollen tube function -the response to the female attraction cue- appeared to be comparable between both pollen tubes due to the wavy pollen tube response to the LURE1 attractant peptide (**Fig. 3C**; Takeuchi and Higashiyama 2016). In the *NASPpro::NASP-mRuby2* ovule, NASP-mRuby2 protein was detected in the nuclei of the egg, central and synergid cells (**Fig. 3D**). However, *nasp*^{cri} mutant female gametophyte cells appeared to be normal in terms of the cell morphology and the expression of cell specification markers (**Fig. 3E**). These observations suggest that the *nasp*^{cri} mutation does not have a major impact on male and female development and function. This was supported by a reciprocal crossing experiment between *GCH3* and *nasp*^{cri}/*NASP GCH3* plants, in which no significant reduction in *nasp*^{cri} transmission from male (45.9%, $n = 220$) and female (57.9%, $n = 164$) was observed. Therefore, the observed phenotype in embryogenesis (**Fig. 2**) could be attributed to the recessive effects of *nasp*^{cri} *GCH3* after fertilization.

NASP is required for early embryo development after the first zygotic division of the *A. thaliana* GFP-CENH3 line

To clarify the contribution of NASP to embryogenesis and CENH3 deposition after fertilization, we used *GCH3* plant lines with homozygous *nasp*^{cri} mutation complemented with

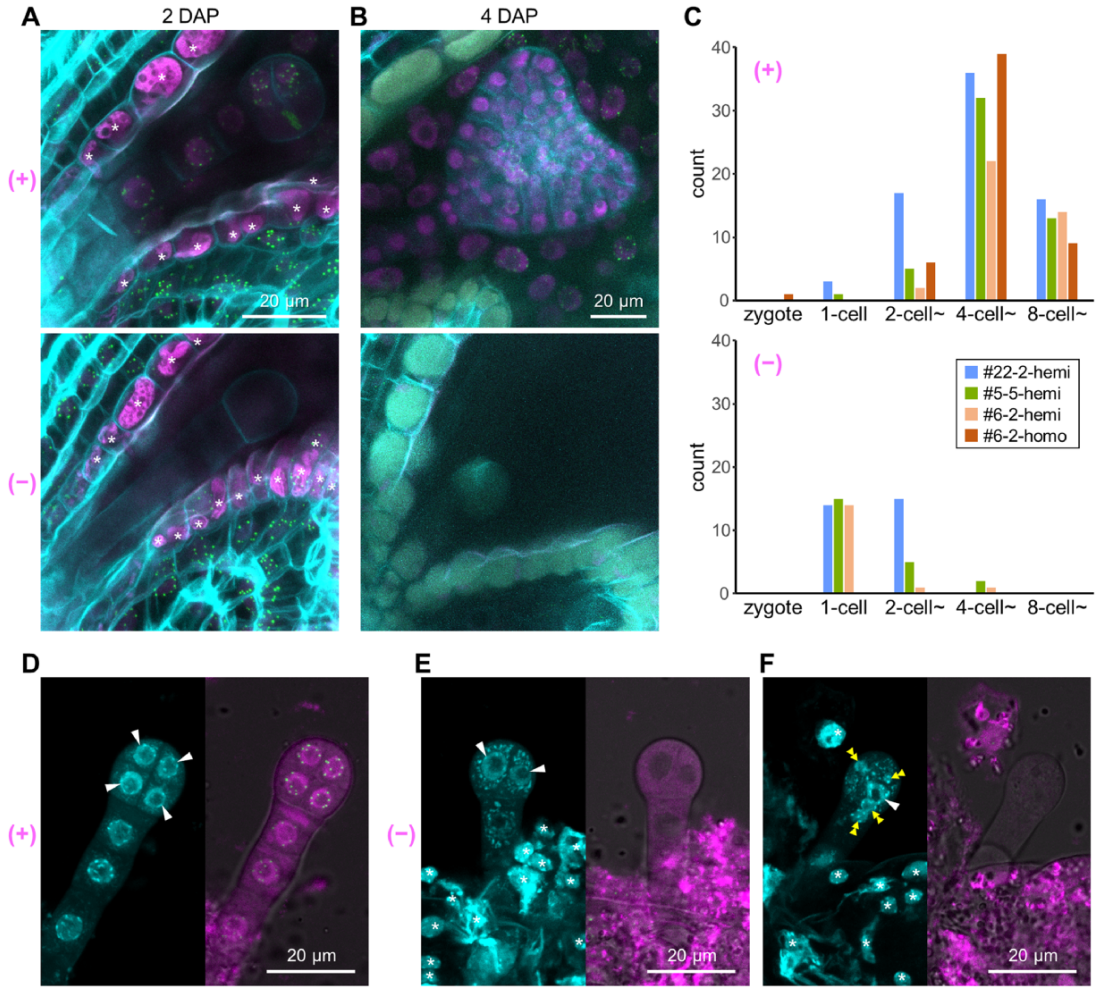

Fig. 4 NASP requirement for early embryogenesis and de novo CENH3 deposition in the *GCH3* line. (A and B) Confocal images of ClearSee-treated embryos inside the ovule at 2 DAP (A) and 4 DAP (B) of a plant line *nasp*^{cri}/*nasp*^{cri} *GCH3* with a hemizygous *NASPpro::NASP-mRuby2* transgene (#6–2-hemi). The presence (+) or absence (−) of mRuby2 fluorescence (shown as magenta) in embryo nuclei indicate NASP-complemented embryo or homozygous *nasp*^{cri} mutant embryo, respectively. The GFP-CENH3 signals (shown as green) at centromeres were observed in the embryo and endosperm of NASP-mRuby2-positive (+) ovules and in the maternal integuments of ovules, independent of the presence of NASP-mRuby2 in embryo cells (+ and −). Note that asterisks indicate unrelated objectives with autofluorescence in ovule integument cells. Cell wall staining with calcofluor white is shown in cyan. (C) The number of ovules with each zygote/embryo stage from three independent hemizygous lines and one homozygous line for *NASPpro::NASP-mRuby2* transgene in homozygous *nasp*^{cri} *GCH3*. Counting was performed using confocal images of ClearSee-treated ovules ($n = 54–101$) from three siliques at 2 DAP. (D–F) Confocal images of 2 DAP embryos pushed out from the ovule tissue in a plant line *nasp*^{cri}/*nasp*^{cri} *GCH3* with a hemizygous *NASPpro::NASP-mRuby2* transgene (#6–2-hemi). Cyan (left panel), Hoechst 33342 staining; green and magenta (right panel), GFP-CENH3 and NASP-mRuby2, respectively. White arrowheads and yellow double arrowheads indicate nuclei with round and normal size and disorganized small nuclei (micronuclei), respectively, in the embryo proper. Asterisks in cyan images indicate nuclei of ovule integument cells.

hemizygous *NASPpro::NASP-mRuby2* transgene. By observing red fluorescence of NASP-mRuby2 at the nucleus, we were able to distinguish whether zygotes and early embryos in self-pollinated pistils consisted of cells of functional *NASP* (homozygous or hemizygous *NASPpro::NASP-mRuby2*) or *nasp*^{cri} *GCH3* mutant (**Fig. 4**). At 2 d after pollination (2 DAP), most NASP-mRuby2-positive embryos normally developed at the four- or eight-cell stage, whereas NASP-mRuby2-negative ones were at the one- or two-cell stage (**Fig. 4A, C**). At 4 DAP, NASP-mRuby2-positive embryos further developed to about the early-heart stage without any obvious morphological defects, whereas NASP-mRuby2-negative ones were still at the one- or two-cell stage (**Fig. 4B**). Normally developing NASP-mRuby2-positive embryo cells exhibited GFP-CENH3 signals, while the NASP-mRuby2-negative embryo cells had no GFP-CENH3 signals in the nucleus (**Fig. 4A, B**).

To investigate whether the absence of NASP affects nuclear organization, 2 DAP embryos were squeezed out from the ovule and into a staining solution containing the DNA dye Hoechst 33342 (Kurihara et al. 2015, Musielak et al. 2015). In control NASP-mRuby2-positive embryos typically at the four- or eight-cell stage, we observed nuclear DNA staining with small

brighter signals indicative of chromocenters as well as organellar DNA staining (**Fig. 4D**). Most NASP-mRuby2-negative embryos at the one- or two-cell stage were similarly stained with the DNA dye (**Fig. 4E**). Interestingly, some of the NASP-mRuby2-negative embryos contained disorganized small nuclei, so-called micronuclei (**Fig. 4F**), suggesting that the absence of functional NASP caused a chromosome mis-segregation event due to the failure of CENH3 deposition in the zygote and one-cell stage embryo.

Species-specific sequences of NASP determine its function in embryogenesis

Taking advantage of the *nasp*^{cri}/*NASP GCH3* line that showed the clear embryogenesis phenotype (**Fig. 2C, E**), we assessed the importance of NASP protein and its domains in terms of species-specific amino acid sequences by complementation testing. Similar to the assessment for CENH3, as shown in **Fig. 1**, we focused on NASP from *A. thaliana*, the *Brassicaceae* species - *Capsella rubella*, *Z. mays* and *M. polymorpha*. The abnormal seed phenotype of *nasp*^{cri}/*NASP GCH3* was restored in some T1 lines with the introduction of *AtNASP* and *CrNASP* coding sequences, similar to *AtNASP* genomic sequence, whereas it was not in any of the T1 lines for *ZmNASP* and *MpNASP* (**Fig. 2D**), suggesting that NASP requires a certain degree of species-specific amino acid sequence for its function.

We compared amino acid sequences of NASP from human and in these four plant species (**Fig. 5A**). NASP proteins include four TPR motifs and a C-terminal extension containing a nuclear localization signal (Dunleavy et al. 2007, Bowman et al. 2015, Liu et al. 2021, 2022, Bao et al. 2022). The NASPs contain an acidic amino acid–rich stretch as an interrupted loop in the second TPR, which seems to be variable between species, and a less conserved N-terminal region without any predicted protein structures (**Fig. 5A**). To examine the requirement of each NASP region for its function in *A. thaliana* embryogenesis, we introduced AtNASP variants fused with the cyan fluorescent protein mTurquoise2 into *nasp*^{cri}/*NASP GCH3*. Compared with the control full-length wild-type AtNASP (*At*), AtNASP lacking the N-terminal region [*At* (ΔN)] complemented the abnormal seed phenotype to a lower frequency and degree, and AtNASP lacking the acidic region [*At* (ΔDE)] failed to complement altogether (**Fig. 5B**). Some T1 lines of AtNASP having the N-terminal region of MpNASP [*At* (N^{Mp})] just slightly decreased the abnormal seed phenotype, while more than half of AtNASP T1 lines having the acidic region of MpNASP [*At* (DE^{Mp})] restored the phenotype similar to wild-type AtNASP (**Fig. 5B**). Consistent with this, the abnormal embryo phenotype was restored by the introduction of *At* (DE^{Mp}) but not *At* (N^{Mp}) or MpNASP (*Mp*) (**Fig. 5C**). This analysis suggests that the acidic region is required for NASP function. Our observations are also consistent with the importance of the acidic region of human NASP for binding to H3 to make a complex with H3–H4–ASF1 (Bowman et al. 2017).

A. thaliana NASP interacts with CENH3 through lineage-specific sequence contexts

Our complementation test implied the requirement of lineage-specific sequence contexts for NASP function. Since amino acid sequences of canonical histone H3 are identical among land plant species (**Supplementary Fig. S1A**), we postulated that the lineage-specific NASP–CENH3 interaction could explain the functionality of NASP variants. To assess whether CENH3 variants, including a chimera of AtCENH3 and MpCENH3, interacted with AtNASP, we performed a semi-quantitative interaction assay using the BiFC assay in *N. benthamiana* leaf epidermal cells. As a control, we also assessed the interaction between CENH3 variants and *A. thaliana* ASF1A, a conserved histone chaperone for H3/H4 (Zhu et al. 2011, Min et al. 2019, Zhong et al. 2022).

In our BiFC assay employing the P2A-NLS-mCherry (PNC) module, as used in **Fig. 1**, YFP fluorescence (BiFC signal) is observed if AtASF1A or AtNASP fused to nYFP interacts with H3.3 or CENH3 variants fused to cYFP-PNC, while mCherry fluorescence certifies the comparable translation level of H3.3 or CENH3 variants (**Fig. 6**). The BiFC assay indicated that AtASF1A interacts with both AtCENH3 and MpCENH3, but that AtNASP only interacts with conspecific AtCENH3 (**Fig. 6A**). AtASF1A interacted with H3.3, ZmCENH3 and all the At/Mp-chimeric CENH3 variants we tested, despite slight differences in relative BiFC intensities (**Fig. 6B**). In contrast, AtNASP interacted with AtCENH3, ZmCENH3 and some chimeric CENH3 variants but not with the others or MpCENH3 (**Fig. 6C**). When a single region, either LoopN-α1 (block 3) or α2 (block 5) of AtCENH3, which were required for targeting to *A. thaliana* centromeres (**Fig. 1D**), was swapped with that of MpCENH3, these chimeric CENH3 variants retained the interaction capability with AtNASP (**Fig. 6C**, i). The introduction of block 3 or blocks 3 plus 5 from AtCENH3 into the MpCENH3 framework did not confer the interaction capability (**Fig. 6C**, ii). Interestingly, CENH3 variants with blocks 1/2/3 or blocks 2/3/4 of AtCENH3 interacted with AtNASP, while CENH3 variants with the same blocks of MpCENH3 did not (**Fig. 6C**, iii). This clear contrast demonstrates that the NASP–CENH3 interaction relies on angiosperm-specific sequence contexts of CENH3 αN and LoopN-α1. Together with the result that the LoopN-α1 region of AtCENH3 plays a dominant role in the centromere targeting of *A. thaliana* and tobacco BY-2 cells (**Fig. 1**, **Supplementary Fig. S2** and **S3**), our data suggest that NASP can recognize CENH3 through the LoopN-α1 region and escort it into the nucleoplasm for deposition on the centromere nucleosome.

A previous study using structural and biochemical approaches for AtNASP and canonical H3 showed that AtNASP has two distinct sets of amino acid clusters for in vitro binding to the H3 N-terminal (a.a. 21–59 containing αN) and α3 (a.a. 116–135) regions, respectively (Liu et al. 2022, **Fig. 5A**, **Supplementary Fig. S1C, D**), similar to the binding mode of human NASP to H3 (Bowman et al. 2017, Liu et al. 2021, Bao et al. 2022). Although this applies to the canonical H3, AtNASP might also bind to CENH3 via these regions, which are not completely

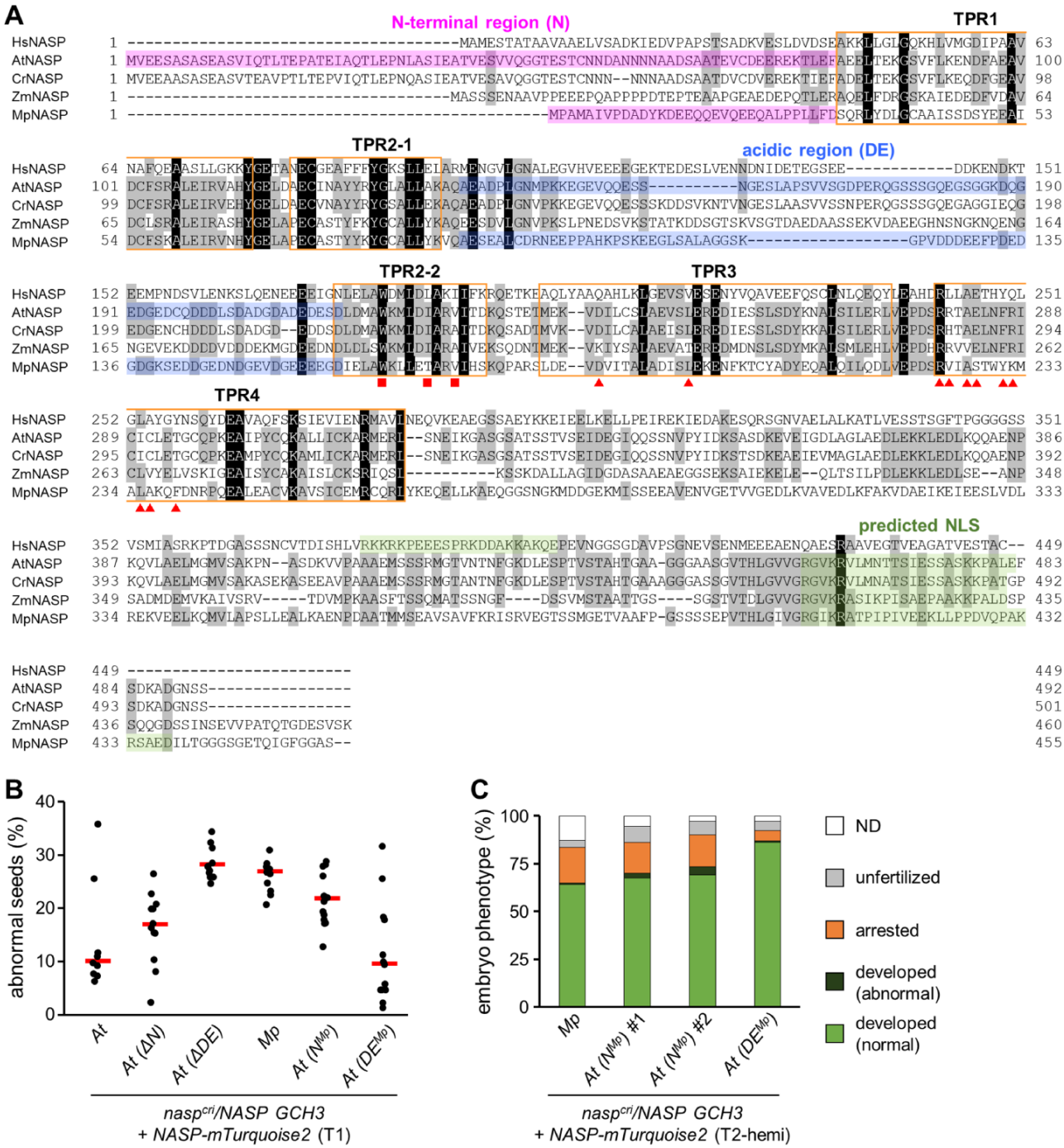

Fig. 5 NASP protein domains required for the function in *A. thaliana* embryo development. (A) Sequence alignment of NASP proteins from *H. sapiens* (HsNASP), *A. thaliana* (AtNASP), *Z. mays* (ZmNASP) and *M. polymorpha* (MpNASP). Squares and triangles below the alignment indicate amino acids of AtNASP that have been shown to mediate binding to canonical H3's N-terminal and α3 regions, respectively (Liu et al. 2022). See also **Supplementary Fig. S1C** and **D** for sequence alignments of these binding regions of H3 compared to AtCENH3 and MpCENH3. (B) The percentage of abnormal seeds per developing seeds in self-pollinated siliques for transgenic lines with the *nasp*^{cri}/*NASP* genotype. Each dot represents the value for each independent T1 plant. Red bars indicate median values. Approximately 200 developing seeds were counted from five siliques. (C) The proportion of embryo phenotype. The phenotype was categorized as noted for **Fig. 2F**. A total of 101–246 ovules/seeds from three to seven siliques were analyzed for each genotype.

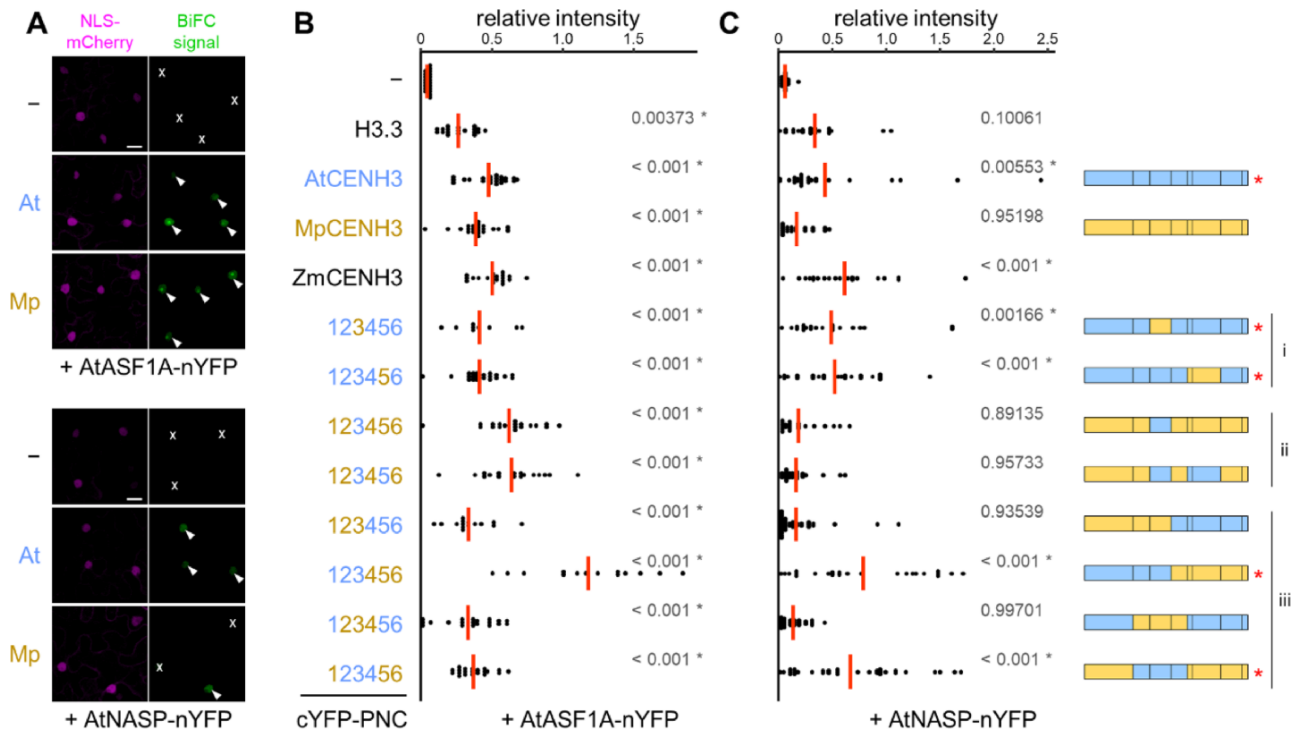

Fig. 6 Interaction assay for CENH3 variants and AtASF1A or AtNASP using a BiFC system with the PNC module. (A) Confocal images of *N. benthamiana* leaf epidermal cells of the BiFC assay between AtASF1A-nYFP or AtNASP-nYFP and cYFP-PNC (–), AtCENH3-cYFP-PNC (At) or MpCENH3-cYFP-PNC (Mp). Equivalent NLS-mCherry signal indicates comparable levels of the three cYFP fusion proteins. Nuclei with negative or positive BiFC signals are marked with × or arrowheads, respectively. Scale bars, 20 μm. (B and C) The relative BiFC intensity (BiFC/mCherry) for H3.3, AtCENH3, MpCENH3, ZmCENH3 or At/Mp-chimeric CENH3 variants with AtASF1A (B) and AtNASP (C). Each dot represents the value of the individual nuclei. Short lines on the dot show the mean of the values. *P* values are estimated by Dunnett's test compared to the negative control (–). For AtCENH3, MpCENH3 and At/Mp-chimeric CENH3 variants, block bars on the right indicate the structure of each variant with colors (light blue, AtCENH3; yellow, MpCENH3), and red asterisks indicate CENH3 variants with significant BiFC signal.

conserved between AtCENH3 and MpCENH3 (**Supplementary Fig. S1C, D**). Since our interaction assay using *N. benthamiana* implies that AtNASP requires AtCENH3's LoopN-α1 in addition to αN, but not α3, for the species-specific NASP–CENH3 interaction (**Fig. 6C**), the recognition of CENH3 by NASP could be mediated by different dynamics *in planta*. Altogether, our results indicated that NASP acts as a key chaperone that binds CENH3 in a species-specific manner in plants. The fact that the fully arrested embryonic phenotype of the *nasp* mutant in the *GCH3* background was masked in the wild-type background implicates some other important components for the normal CENH3 supply network (that might be fastidious for the GFP tag of CENH3), including another general H3 chaperone, ASF1 (**Fig. 6B**, Cook et al. 2011). In combination with the NASP–CENH3 function, it would also be interesting to study other epigenetic marks and regulators, such as other histone H3 chaperones, CAF1 and HIRA complexes (Nie et al. 2014, Duc et al. 2017, Jiang and Berger 2017b), involved in gametophyte functions and embryogenesis.

Conclusions

In this study, we defined *A. thaliana* CENH3 domains that are important for centromere targeting and identified NASP as a chaperone that binds CENH3 through a domain around LoopN-α1 in a species-specific sequence manner. In addition, we demonstrated that NASP is involved in early embryo development and CENH3 deposition after fertilization. Although NASP seems to be neither a CENH3-specific chaperone nor a sole chaperone that recognizes CENH3, we hypothesize that NASP contributes to the de novo deposition of CENH3 on the centromere after fertilization. This function requires species-specific sequences, suggesting the coevolution of NASP with CENH3 after fertilization. Our findings help to understand how the CENH3 protein is deposited at the centromere in the zygote nucleus, which may contribute to haploid induction technology by manipulation of the CENH3 deposition network.

Materials and Methods

Plant materials

Arabidopsis thaliana Col-0 was used for the expression and localization experiment of CENH3 variants. The *GFP-CENH3* in *cenh3-1* (*GCH3*) line was kindly provided by Dr. Simon Chan's laboratory (University of California, Davis, CA, USA) (Ravi et al. 2010). For transformation of *A. thaliana* plants, T-DNA constructs were introduced by floral dip using *Agrobacterium tumefaciens* strain GV3101. *Arabidopsis thaliana* plants were germinated on half-strength Murashige-Skoog solid medium containing antibiotics (if applicable) under continuous light at

22°C and transferred on soil for further growth under long-day condition in plant growth rooms. *N. benthamiana* plants were grown from directly sowing seeds on soil in plant growth rooms under long-day conditions at 22–26°C. Transformation of tobacco BY-2 cultured cells was performed as previously described (Mayo et al. 2006) using *A. tumefaciens* strain EHA105. Several transformants per construct were selected via several rounds of subculturing of callus on modified Linsmaier-Skoog (LS) medium containing 1.5% agar, 50 mg/l kanamycin and 100 mg/l cefotaxime sodium. Each BY-2 callus was observed by suspending in liquid modified LS medium.

Plasmids and sequences

All plasmids were generated by standard molecular techniques and are listed in **Supplementary Table S1**. The PNC sequence was amplified from a plasmid obtained from Dr. Tomokazu Kawashima (Kawashima et al. 2014). The *nasp*^{cri} mutant was generated by the CRISPR/Cas9 system based on pKIR1.1 (Tsutsui and Higashiyama 2017). Gene and protein sequence data can be obtained from The Arabidopsis Information Resource (http://arabidopsis.org) for *A. thaliana* and from Phytozome (https://phytozome-next.jgi.doe.gov/) for *C. rubella*, *Z. mays* and *M. polymorpha*.

Confocal microscopy and image analysis

Confocal images of petal cells, ovules and BY-2 cells of transgenic lines were taken using an LSM-780-DUO-NLO system (Zeiss, Oberkochen, Germany). Images were acquired using ZEN 2010 software (Zeiss) and processed using Fiji software (http://fiji.sc/Fiji).

Establishment of the *nasp*^{cri} Mutant Line

The *GCH3* plant was transformed with HTv985, pKIR1.1 vector containing the guide RNA (gRNA) sequence (5′-GTCGAATCGGTTGTTCAGGG-3′) that targets the first exon of *NASP* gene (**Fig. 2A**), and resulting T1 seeds were selected by red fluorescence of seeds. One mutant candidate (#3) was obtained by genomic PCR using primers [NASP + 3 F (5′-GGTTGAAGAATCAGCTTC-3′) and NASP + 440 R (5′-CATGATTAGATCATTCGAG-3′)] and direct Sanger sequencing, which showed a disrupted sequence around the gRNA target site. From seeds harvested from this candidate T1 individual, Cas9-free plants were selected based on the absence of red fluorescence of seeds and confirmed later by no hygromycin-resistant seedling in the next generation. Genomic PCR and sequencing analysis identified the 10-bp deletion in the *nasp*^{cri}/*NASP GCH3* line (#3–16). The siblings from the #3-16 line plants were used for phenotypic analysis and transformation for complementation tests. The *nasp*^{cri}/*NASP GCH3* was backcrossed several times to wild-type Col-0 or FGR8.0 (Völz et al. 2013) to remove the *GFP-CENH3* transgene and the *cenh3-1* mutant allele.

Based on the 10-bp deletion, NASP + 141 R (5′-AGTGCCTCCCTGAACA AC-3′) for wild-type *NASP* and nasp^{cri} F (5′-CGTCGAATCGGAGGCA-3′) for 10-bp deletion *nasp*^{cri} allele were designed (**Fig. 2B**). Primers for wild-type allele [NASP-1162F (5′-AATACTAAGCGAGCCATC-3′) and NASP + 141R] and primers for *nasp*^{cri} allele (nasp^{cri} F and NASP + 440R) were used to exclusively amplify endogenous *NASP* gene and *nasp*^{cri} allele, respectively.

Evaluation of the embryo phenotype by clearing in chloral hydrate solution

The carpel walls were removed from siliques 5 d after hand pollination using tweezers and 27-gauge needle (Terumo, Tokyo, Japan). The remaining tissues, ovules/seeds attached to the septum, were fixed and decolorized in ethanol/acetic acid (9:1) and rehydrated with ethanol series (80%, 60%, 40% and 20%) and distilled water. After rehydration, the samples were cleared in chloral hydrate solution (chloral hydrate, glycerol and distilled water in the weight ratio of 8:1:3). Differential interference contrast microscopy analysis of cleared ovules/seeds was performed using a Nikon Ts2R microscope.

Evaluation of embryo development with fluorescence

To observe GFP-CENH3 and NASP-mRuby2 fluorescence of embryo cells in the early developing seed, the ClearSee method was used in combination with cell wall staining. Two or four days after hand pollination, siliques were dissected as described earlier and fixed by immersing in 4% paraformaldehyde/PBS and applying a reduced pressure with a vacuum pump. About 1 h after the fixation, samples were washed with PBS twice and cleared with ClearSeeAlpha solution to reduce the formation of brown pigments in the ClearSee-treated ovule (Kurihara et al. 2021). Two to three weeks after treatment in the dark at room temperature, the samples were stained with ClearSee solution (Kurihara et al. 2015) containing 0.1 mg/ml calcofluor white for 1 h and then washed with ClearSee solution for 1 h. The silique sample was split at the center of the septum to separate two lines of placenta with seeds into one line of that, which facilitates the observation of embryo phenotype without overlapping each seed tissue.

To observe the nuclei of embryo cells, the direct staining method was used with a staining solution (4% paraformaldehyde/PBS, 1% DMSO, 0.05% Triton-X100, 5% glycerol) in combination with 10 μg/ml Hoechst 33342 (Kurihara et al. 2015, Musielak et al. 2015). Early developing seeds in 2 DAP siliques were dissected into the solution on a microscope slide, and embryos were pushed out from the maternal tissue using a coverslip.

For confocal observation using the LSM-780-DUO-NLO system (Zeiss), images were acquired with a 40× objective lens (LD C-Apochromat 40×/1.1 W Corr, Zeiss) under excitation wavelengths of 488/561 nm and emission wavelengths of 490–561/588–695 nm for mClover and mRuby2 fluorescence and sequentially under an excitation wavelength of 405 nm and emission wavelengths of 415–490 nm for calcofluor white.

Pollen viability staining

Pollen viability in the anther was assessed by chemical staining (Peterson et al. 2010, Motomura et al. 2020), with slight modifications. Briefly, flowers before anthesis were fixed in ethanol/acetic acid (7:3) and stained with a staining solution (10% ethanol, 0.01% malachite green, 25% glycerol, 0.05% acid fuchsin, 0.005% orange G and 4% acetic acid). Stamens were dissected from the stained sample and observed by light microscopy using a Nikon Ts2R microscope.

BiFC assay

Transient expression in *N. benthamiana* leaves by agroinfiltration was performed as previously described (Takeuchi and Higashiyama 2016). Equal amounts of *A. tumefaciens* strain GV3101 cultures for nYFP and cYFP-PNC constructs and the p19 silencing suppressor were collected in a tube and resuspended in infiltration buffer (10 mM $MgCl_2$, 10 mM MES, pH 5.6 and 150 μM acetosyringone). Three to four hours after incubation at 26°C, the mixed suspensions were infiltrated in four to 5-week-old *N. benthamiana* leaves. Two days after infiltration, the leaf samples were subjected to confocal microscope observation using the LSM-780-DUO-NLO system (Zeiss).

To virtually normalize protein production levels among CENH3 variants fused to the cYFP-PNC sequence, the relative BiFC intensity was the BiFC signal (YFP fluorescence) divided by the NLS-mCherry signal. For each channel of images, the background was subtracted and the fluorescence intensity of nuclei regions was measured. For each BiFC combination, the relative intensity of 9–36 nuclei from three replicate samples was calculated and plotted using R studio (https://cran.ism.ac.jp/). Statistical analysis was also performed using R studio ('multcomp' package; https://CRAN.R-project.org/package=multcomp) based on Dunnett's multiple comparison test.

Supplementary Data

Supplementary data are available at *PCP* online.

Data Availability

The data underlying this study, including nucleotide and protein sequences, are available in the article and supplementary data.

Funding

The Japan Society for the Promotion of Science on Overseas Research Fellowship (No. 27-601), Grant-in-Aid for Scientific Research on Innovative Areas (18H04834) and the Sumitomo Foundation Grant for Basic Science Research Projects (170663) (to H.T.); Grant-in-Aid for Scientific Research on Innovative Areas, Advanced Bioimaging Support (16H06280, 22H04926); and The Austrian Science Fund (to F.B.) (I 2163, P28320).

Acknowledgments

We thank Simon Chan's laboratory for *GFP-CENH3 in cenh3-1* seeds; Hiroki Tsutsui for pKIR1.1 vector; Tomokazu Kawashima for plasmids and cDNAs used for plasmid construction; Akihisa Osakabe and other members of Berger lab (GMI, Vienna, Austria) for helpful discussion; Daisuke Kurihara for technical assistance of BY-2 experiment; Minako Ueda for technical advice on observation of zygote and early embryo; and Yoshikatsu Sato and Nagoya University Live Imaging Center for the Zeiss LSM-780-DUO-NLO microscope system.

Author Contributions

H.T. conceived and designed this study under the supervision of F.B.; H.T. generated the research materials; H.T. and S.N. performed the experiments and analyzed the data; H.T. wrote the manuscript with input from S.N., T.H. and F.B.

Disclosures

No conflicts of interest declared.

References

Bao, H., Carraro, M., Flury, V., Liu, Y., Luo, M., Chen, L., et al. (2022) NASP maintains histone H3-H4 homeostasis through two distinct H3 binding modes. *Nucleic Acids Res*. 50: 5349–5368.

Barnhart, M.C., Kuich, P.H.J.L., Stellfox, M.E., Ward, J.A., Bassett, E.A., Black, B.E., et al. (2011) HJURP is a CENP-A chromatin assembly factor sufficient to form a functional de novo kinetochore. *J. Cell Biol*. 194: 229–243.

Bassett, E.A., DeNizio, J., Barnhart-Dailey, M.C., Panchenko, T., Sekulic, N., Rogers, D.J., et al. (2012) HJURP uses distinct CENP-A surfaces to recognize and to stabilize CENP-A/histone H4 for centromere assembly. *Dev. Cell* 22: 749–762.

Black, B.E., Jansen, L.E.T., Maddox, P.S., Foltz, D.R., Desai, A.B., Shah, J.V., et al. (2007) Centromere identity maintained by nucleosomes assembled with histone H3 containing the CENP-A targeting domain. *Mol. Cell* 25: 309–322.

Borg, M., Jiang, D. and Berger, F. (2021) Histone variants take center stage in shaping the epigenome. *Curr. Opin. Plant Biol*. 61: 101991.

Bowman, A., Koide, A., Goodman, J.S., Colling, M.E., Zinne, D., Koide, S., et al. (2017) sNASP and ASF1A function through both competitive and compatible modes of histone binding. *Nucleic Acids Res*. 45: 643–656.

Bowman, A., Lercher, L., Singh, H.R., Zinne, D., Timinszky, G., Carlomagno, T., et al. (2015) The histone chaperone sNASP binds a conserved peptide motif within the globular core of histone H3 through its TPR repeats. *Nucleic Acids Res*. 44: 3105–3117.

Camahort, R., Li, B., Florens, L., Swanson, S.K., Washburn, M.P. and Gerton, J.L. (2007) Scm3 is essential to recruit the histone H3 variant Cse4 to centromeres and to maintain a functional kinetochore. *Mol. Cell* 26: 853–865.

Campos, E.I., Fillingham, J., Li, G., Zheng, H., Voigt, P., Kuo, W.H.W., et al. (2010) The program for processing newly synthesized histones H3.1 and H4. *Nat. Struct. Mol. Biol*. 17: 1343–1351.

Chen, C.C., Dechassa, M.L., Bettini, E., Ledoux, M.B., Belisario, C., Heun, P., et al. (2014) CAL1 is the Drosophila CENP-A assembly factor. *J. Cell Biol*. 204: 313–329.

Cho, U.S. and Harrison, S.C. (2011) Recognition of the centromere-specific histone Cse4 by the chaperone Scm3. *Proc. Natl. Acad. Sci. U.S.A*. 108: 9367–9371.

Cook, A.J.L., Gurard-Levin, Z.A., Vassias, I. and Almouzni, G. (2011) A specific function for the histone chaperone NASP to fine-tune a reservoir of soluble H3-H4 in the histone supply chain. *Mol. Cell* 44: 918–927.

Duc, C., Benoit, M., Détourné, G., Simon, L., Poulet, A., Jung, M., et al. (2017) Arabidopsis ATRX modulates H3.3 occupancy and fine-tunes gene expression. *Plant Cell* 29: 1773–1793.

Dunleavy, E.M., Pidoux, A.L., Monet, M., Bonilla, C., Richardson, W., Hamilton, G.L., et al. (2007) A NASP (N1/N2)-related protein, Sim3, Binds CENP-A and is required for its deposition at fission yeast centromeres. *Mol. Cell* 28: 1029–1044.

Dunleavy, E.M., Roche, D., Tagami, H., Lacoste, N., Ray-Gallet, D., Nakamura, Y., et al. (2009) HJURP is a cell-cycle-dependent maintenance and deposition factor of CENP-A at centromeres. *Cell* 137: 485–497.

Filipescu, D., Szenker, E. and Almouzni, G. (2013) Developmental roles of histone H3 variants and their chaperones. *Trends Genet*. 29: 630–640.

Finn, R.M., Ellard, K., Eirín-López, J.M. and Ausió, J. (2012) Vertebrate nucleoplasmin and NASP: egg histone storage proteins with multiple chaperone activities. *FASEB J*. 26: 4788–4804.

Foltz, D.R., Jansen, L.E.T., Bailey, A.O., Yates, J.R., Bassett, E.A., Wood, S., et al. (2009) Centromere-specific assembly of CENP-A nucleosomes is mediated by HJURP. *Cell* 137: 472–484.

Henikoff, S. and Dalal, Y. (2005) Centromeric chromatin: what makes it unique?. *Curr. Opin. Genet. Dev*. 15: 177–184.

Hirsch, C.D., Wu, Y., Yan, H. and Jiang, J. (2009) Lineage-specific adaptive evolution of the centromeric protein cenh3 in diploid and allotetraploid oryza species. *Mol. Biol. Evol*. 26: 2877–2885.

Ingouff, M., Rademacher, S., Holec, S., Šoljić, L., Xin, N., Readshaw, A., et al. (2010) Zygotic resetting of the HISTONE 3 variant repertoire participates in epigenetic reprogramming in arabidopsis. *Curr. Biol*. 20: 2137–2143.

Jiang, D. and Berger, F. (2017a) Histone variants in plant transcriptional regulation. *Biochim. Biophys. Acta - Gene. Regul. Mech*. 1860: 123–130.

Jiang, D. and Berger, F. (2017b) DNA replication–coupled histone modification maintains polycomb gene silencing in plants. *Science* 357: 1146–1149.

Karimi-Ashtiyani, R., Ishii, T., Niessen, M., Stein, N., Heckmann, S., Gurushidze, M., et al. (2015) Point mutation impairs centromeric CENH3 loading and induces haploid plants. *Proc. Natl. Acad. Sci. U.S.A*. 112: 11211–11216.

Kawashima, T., Lorković, Z.J., Nishihama, R., Ishizaki, K., Axelsson, E., Yelagandula, R., et al. (2015) Diversification of histone H2A variants during plant evolution. *Trends Plant Sci*. 20: 419–425.

Kawashima, T., Maruyama, D., Shagirov, M., Li, J., Hamamura, Y., Yelagandula, R., et al. (2014) Dynamic F-actin movement is essential for fertilization in Arabidopsis thaliana. *Elife* 3: 1–18.

Khorasanizadeh, S. (2004) The nucleosome. *Cell* 116: 259–272.

Kuppu, S., Ron, M., Marimuthu, M.P.A., Li, G., Huddleson, A., Siddeek, M.H., et al. (2020) A variety of changes, including CRISPR/Cas9-mediated deletions, in CENH3 lead to haploid induction on outcrossing. *Plant Biotechnol. J*. 18: 2068–2080.

Kurihara, D., Mizuta, Y., Nagahara, S. and Higashiyama, T. (2021) ClearSeeAlpha: advanced optical clearing for whole-plant imaging. *Plant Cell Physiol*. 62: 1302–1310.

Kurihara, D., Mizuta, Y., Sato, Y. and Higashiyama, T. (2015) ClearSee: a rapid optical clearing reagent for whole-plant fluorescence imaging. *Development* 142: 4168–4179.

Le Goff, S., Keçeli, B.N., Jeřábková, H., Heckmann, S., Rutten, T., Cotterell, S., et al. (2020) The H3 histone chaperone NASP SIM3 escorts CenH3 in Arabidopsis. *Plant J*. 101: 71–86.

Lermontova, I., Schubert, V., Fuchs, J., Klatte, S., Macas, J. and Schubert, I. (2006) Loading of Arabidopsis centromeric histone CENH3 occurs mainly during G2 and requires the presence of the histone fold domain. *Plant Cell* 18: 2443–2451.

Liu, C.P., Jin, W., Hu, J., Wang, M., Chen, J., Li, G., et al. (2021) Distinct histone H3-H4 binding modes of sNASP reveal the basis for cooperation and competition of histone chaperones. *Genes Dev*. 35: 1610–1624.

Liu, Y., Chen, L., Wang, N., Wu, B., Bao, H. and Huang, H. (2022) Structural basis for histone H3 recognition by NASP in Arabidopsis. *J. Integr. Plant Biol*. 64: 2309–2313.

Liu, Z., Chen, O., Wall, J.B.J., Zheng, M., Zhou, Y., Wang, L., et al. (2017) Systematic comparison of 2A peptides for cloning multi-genes in a polycistronic vector. *Sci. Rep*. 7: 1–9.

Luger, K., Mä Der, A.W., Richmond, R.K., Sargent, D.F. and Richmond, T.J. (1997) Crystal structure of the nucleosome core particle at 2.8 A resolution. *Nature* 389: 251–260.

Maheshwari, S., Ishii, T., Brown, C.T., Houben, A. and Comai, L. (2017) Centromere location in Arabidopsis is unaltered by extreme divergence in CENH3 protein sequence. *Genome Res*. 27: 471–478.

Maheshwari, S., Tan, E.H., West, A., Franklin, F.C.H., Comai, L. and Chan, S.W.L. (2015) Naturally occurring differences in CENH3 affect chromosome segregation in zygotic mitosis of hybrids. *PLoS Genet*. 11: 1–20.

Maksimov, V., Nakamura, M., Wildhaber, T., Nanni, P., Ramström, M., Bergquist, J., et al. (2016) The H3 chaperone function of NASP is conserved in Arabidopsis. *Plant J*. 88: 425–436.

Malik, H.S. and Henikoff, S. (2009) Major Evolutionary Transitions in Centromere Complexity. *Cell* 138: 1067–1082.

Malik, H.S., Vermaak, D. and Henikoff, S. (2002) Recurrent evolution of DNA-binding motifs in the Drosophila centromeric histone. *Proc. Natl. Acad. Sci. U.S.A*. 99: 1449–1454.

Marimuthu, M.P.A., Maruthachalam, R., Bondada, R., Kuppu, S., Tan, E.H., Britt, A., et al. (2021) Epigenetically mismatched parental centromeres trigger genome elimination in hybrids. *Sci. Adv*. 7: 1–19.

Mayo, K.J., Gonzales, B.J. and Mason, H.S. (2006) Genetic transformation of tobacco NT1 cells with *Agrobacterium tumefaciens*. *Nat. Protoc*. 1: 1105–1111.

Medina-Pritchard, B., Lazou, V., Zou, J., Byron, O., Abad, M.A., Rappsilber, J., et al. (2020) Structural basis for centromere maintenance by Drosophila CENP – A chaperone CAL 1. *Embo J*. 39: 1–21.

Min, Y., Frost, J.M. and Choi, Y. (2019) Nuclear chaperone ASF1 is required for gametogenesis in Arabidopsis thaliana. *Sci. Rep*. 9: 13959.

Morris, C.A. and Moazed, D. (2007) Centromere assembly and propagation. *Cell* 128: 647–650.

Motomura, K., Arae, T., Araki-Uramoto, H., Suzuki, Y., Takeuchi, H., Suzuki, T., et al. (2020) AtNOT1 is a novel regulator of gene expression during pollen development. *Plant Cell Physiol*. 61: 712–721.

Musielak, T.J., Schenkel, L., Kolb, M., Henschen, A. and Bayer, M. (2015) A simple and versatile cell wall staining protocol to study plant reproduction. *Plant Reprod*. 28: 161–169.

Nagaki, K., Terada, K., Wakimoto, M., Kashihara, K. and Murata, M. (2010) Centromere targeting of alien CENH3s in arabidopsis and tobacco cells. *Chromosom Res*. 18: 203–211.

Naish, M., Alonge, M., Wlodzimierz, P., Tock, A.J., Abramson, B.W., Schmücker, A., et al. (2021) The genetic and epigenetic landscape of the Arabidopsis centromeres. *Science* 374: eabi7489.

Nie, X., Wang, H., Li, J., Holec, S. and Berger, F. (2014) The HIRA complex that deposits the histone H3.3 is conserved in Arabidopsis and facilitates transcriptional dynamics. *Biol. Open* 3: 794–802.

Osakabe, A., Tachiwana, H., Matsunaga, T., Shiga, T., Nozawa, R.S., Obuse, C., et al. (2010) Nucleosome formation activity of human somatic Nuclear Autoantigenic Sperm Protein (sNASP). *J. Biol. Chem*. 285: 11913–11921.

Palladino, J., Chavan, A., Sposato, A., Mason, T.D. and Mellone, B.G. (2020) Targeted *de novo* centromere formation in *Drosophila* reveals plasticity and maintenance potential of CENP-A chromatin. *Dev. Cell* 52: 379–394.e7.

Peterson, R., Slovin, J. and Chen, C. (2010) A simplified method for differential staining of aborted and non-aborted pollen grains. *Int. J. Plant Biol*. 1: e13.

Phansalkar, R., Lapierre, P. and Mellone, B.G. (2012) Evolutionary insights into the role of the essential centromere protein CAL1 in Drosophila. *Chromosom Res*. 20: 493–504.

Pusarla, R.H. and Bhargava, P. (2005) Histones in functional diversification: core histone variants. *FEBS J*. 272: 5149–5168.

Ravi, M. and Chan, S.W.L. (2010) Haploid plants produced by centromere-mediated genome elimination. *Nature* 464: 615–618.

Ravi, M., Kwong, P.N., Menorca, R.M.G., Valencia, J.T., Ramahi, J.S., Stewart, J.L., et al. (2010) The rapidly evolving centromere-specific histone has stringent functional requirements in Arabidopsis thaliana. *Genetics* 186: 461–471.

Ravi, M., Marimuthu, M.P.A., Tan, E.H., Maheshwari, S., Henry, I.M., Marin-Rodriguez, B., et al. (2014) A haploid genetics toolbox for Arabidopsis thaliana. *Nat. Commun*. 5: 1–8.

Richardson, R.T., Alekseev, O.M., Grossman, G., Widgren, E.E., Thresher, R., Wagner, E.J., et al. (2006) Nuclear autoantigenic sperm protein (NASP), a linker histone chaperone that is required for cell proliferation. *J. Biol. Chem*. 281: 21526–21534.

Richardson, R.T., Batova, I.N., Widgren, E.E., Zheng, L.X., Whitfield, M., Marzluff, W.F., et al. (2000) Characterization of the histone H1-binding protein, NASP, as a cell cycle-regulated somatic protein. *J. Biol. Chem*. 275: 30378–30386.

Rosin, L. and Mellone, B.G. (2016) Co-evolving CENP-A and CAL1 domains mediate centromeric CENP-A Deposition across Drosophila species. *Dev. Cell* 37: 136–147.

Rosin, L.F. and Mellone, B.G. (2017) Centromeres drive a hard bargain. *Trends Genet*. 33: 101–117.

Roure, V., Medina-Pritchard, B., Lazou, V., Rago, L., Anselm, E., Venegas, D., et al. (2019) Reconstituting drosophila centromere identity in human cells. *Cell Rep*. 29: 464–479.e5.

Sanei, M., Pickering, R., Kumke, K., Nasuda, S. and Houben, A. (2011) Loss of centromeric histone H3 (CENH3) from centromeres precedes uniparental chromosome elimination in interspecific barley hybrids. *Proc. Natl. Acad. Sci. U.S.A*. 108: E498–505.

Stoler, S., Rogers, K., Weitze, S., Morey, L., Fitzgerald-Hayes, M. and Baker, R.E. (2007) Scm3, an essential Saccharomyces cerevisiae centromere protein required for G2/M progression and Cse4 localization. *Proc. Natl. Acad. Sci. U.S.A*. 104: 10571–10576.

Takeuchi, H. and Higashiyama, T. (2016) Tip-localized receptors control pollen tube growth and LURE sensing in Arabidopsis. *Nature* 531: 245–248.

Talbert, P.B. and Henikoff, S. (2010) Histone variants ancient wrap artists of the epigenome. *Nat. Rev. Mol. Cell Biol* 11: 264–275.

Talbert, P.B. and Henikoff, S. (2017) Histone variants on the move: Substrates for chromatin dynamics. *Nat. Rev. Mol. Cell Biol* 18: 115–126.

Talbert, P.B., Masuelli, R., Tyagi, A.P., Comai, L. and Henikoff, S. (2002) Centromeric localization and adaptive evolution of an Arabidopsis histone H3 variant. *Plant Cell* 14: 1053–1066.

Tsutsui, H. and Higashiyama, T. (2017) pKAMA-ITACHI vectors for highly efficient CRISPR/Cas9-mediated gene knockout in Arabidopsis thaliana. *Plant Cell Physiol*. 58: 46–56.

Völz, R., Heydlauff, J., Ripper, D., von Lyncker, L. and Groß-Hardt, R. (2013) Ethylene signaling is required for synergid degeneration and the establishment of a pollen tube block. *Dev. Cell* 25: 310–316.

Yuan, J., Guo, X., Hu, J., Lv, Z. and Han, F. (2015) Characterization of two CENH3 genes and their roles in wheat evolution. *New Phytol*. 206: 839–851.

Zhang, W., Lee, H.R., Koo, D.H. and Jiang, J. (2008) Epigenetic modification of centromeric chromatin: hypomethylation of DNA sequences in the CENH3-associated chromatin in Arabidopsis thaliana and maize. *Plant Cell* 20: 25–34.

Zhong, Z., Wang, Y., Wang, M., Yang, F., Thomas, Q.A., Xue, Y., et al. (2022) Histone chaperone ASF1 mediates H3.3-H4 deposition in Arabidopsis. *Nat. Commun*. 13: 6970.

Zhou, Z., Feng, H., Zhou, B.R., Ghirlando, R., Hu, K., Zwolak, A., et al. (2011) Structural basis for recognition of centromere histone variant CenH3 by the chaperone Scm3. *Nature* 472: 234–238.

Zhu, Y., Weng, M., Yang, Y., Zhang, C., Li, Z., Shen, W.H., et al. (2011) Arabidopsis homologues of the histone chaperone ASF1 are crucial for chromatin replication and cell proliferation in plant development. *Plant J*. 66: 443–455.